Optimal Kinematic Calibration of the 6-UPS Parallel Manipulator

Genliang Chen, Hao Wang*, and Zhongqin Lin

State Key Laboratory of Mechanical System and Vibration (Shanghai Jiao Tong University), Dongchuan Road 800, Minhang District, 200240 Shanghai, P.R. China
{leungchan,wanghao,zqlin}@sjtu.edu.cn

Abstract. This paper presents the optimal kinematic calibration of the Hexapod (6-UPS) parallel manipulator based on a new observability index. The polytope description, rather than the widely used ellipsoid one, is introduced to depict the inaccuracy of the identified parameters. Then, the infinity-norm of the residual errors is utilized to assess the calibration precision of the kinematic parameters, which should be minimized during the process of measurement configurations selection. In order to find the optimal configurations, the Particle Swarm Optimization (PSO) algorithm is employed in the proposed method and a collision mechanism is added to cope with the joint space boundary constraint of the studied manipulator. In the end, a numerical example is studied to verify the correctness and effectiveness of the proposed approach.

Keywords: Optimal kinematic calibration, Observability index, Particle Swarm Optimization algorithm, Hexapod manipulator.

1 Introduction

Due to the inevitable defects in manufacturing and assembly, the manipulators' kinematic parameters do not exactly match the design goal, which influences the positioning accuracy significantly. Therefore, kinematic calibration is always carried out as an economical and efficient way to overcome this problem by compensating the errored parameters [1]. However, due to the existence of measurement errors, the kinematic parameters cannot be perfectly calibrated. Moreover, the identification precision is sensitive to the sensor noise in some cases.

To minimize the effects of the sensor noise on the calibration quality, much research work has been done in the past few decades, which are mainly concerning their investigations on the determination of the optimal measurement configurations for robot calibration [2]-[7]. Then, the problem can be expressed as to choose a particular set of measurement configurations to minimize some specific observability indices, which are used to evaluate the goodness of the selected configurations. All these indices are derived based on the singular value decomposition (SVD) of the identification matrix $\mathbf{J}_P$ whose inverse linearly transforms the measurement errors to the inaccuracy of the identified parameters.

* Corresponding author.

J. Lee et al. (Eds.): ICIRA 2013, Part I, LNAI 8102, pp. 384–395, 2013.

Borm and Menq [8] selected the geometric mean of all the identification Jacobian matrix's non-zero singular values as the observability index (termed as $O_1 = m^{-\frac{1}{2}}(\delta_1 \cdots \delta_L)^{\frac{1}{L}}$, where $\delta_1, \cdots, \delta_L$ represent the singular values and m is the number of the measured configurations). It can also be related to the determinate of the symmetric matrix $\mathbf{M}_p = \mathbf{J}_P^T \mathbf{J}_P$. Driels and Pathre [2] suggested the condition number of $\mathbf{J}_P$ as the observability index (expressed as $O_2 = \delta_L/\delta_1$). In addition, Nahvi and Hollerbach used the minimal singular value of $\mathbf{J}_P$ (denoted as $O_3 = \delta_L$ [9])) and the multiplication of O_2 and O_3 (namely $O_4 = \delta_L^2/\delta_1$ as the noise amplification index [10]) as the observability indices, respectively. Sun and Hollerbach [11] have systematically compared these observability indices to the alphabet optimalities from experimental design literatures and proposed some useful criteria for observability index option in the light of different purposes.

However, from the viewpoint of optimal experiment design, all these indices are based on the statistics of redundant datum measurements [11]. They just indicate a possibility for estimation precision. No guarantee can be made for the robot's identified parameters that the residual errors are no more than specific quantities, which is important to assess the accuracy performance of robot manipulators.

Otherwise, all the above indices are obtained under the assumption of unit hypersphere constraint for sensor noise, namely $\|\varepsilon \boldsymbol{Y}\|_2 \leq 1$ (where $\varepsilon \boldsymbol{Y}$ is the composed measurement error vector). As a matter of fact, the pose sensor performs the measurements individually at different configurations during the calibration process. Consequently, a hypercube will be generated for the constraint of sensor noise. And an error polytope, rather than the ellipsoid, can be obtained for the identified parameters through the linear mapping with $\mathbf{J}_P$.

For the above reasons, this paper presents a new observability index to evaluate the goodness of the selected measurement configurations for robot calibration. It is derived based on the polytope description of the residual errors and a bounding box is generated to estimate the inaccuracy of the identified parameters. The l_∞-norm of the residual errors, also known as the worst situation of parameter identification, is defined as a new index O_∞ which should be minimized in the optimal configurations selection. The PSO algorithm is introduced and modified to determine the optimal configurations. A collision mechanism is employed into the searching process to cope with the input boundary constraint of the manipulator's actuated joints. With the proposed method, the worst case of parameter identification can be obtained. As a result, the calibration precision of the identified parameters can be guaranteed, which is essential to predict the absolute positioning accuracy of robot manipulators.

The rest of this paper is organized as follows. In Sec.2, the polytope and the ellipsoid descriptions for residual errors are compared via an intuitive example. Then, Sec.3 presents the definition and derivation of the proposed observability index for configuration selection. The PSO algorithm with collision mechanism is introduced in Sec.4 to search for the optimal configurations. In Sec.5, the Hexapod manipulator is studied as a numerical example to verify effectiveness of the proposed method. In the end, some conclusions are drawn in Sec.6.

2 Polytope versus Ellipsoid for Error Description

Generally, the task velocity vector of a robot manipulator in the workspace can be obtained through the linear mapping

$$\dot{\boldsymbol{y}} = \mathbf{J}\dot{\boldsymbol{q}} \tag{1}$$

where $\boldsymbol{q} \in \mathbb{R}^n$ and $\boldsymbol{y} \in \mathbb{R}^m$ denote the input and the output vectors in the robot's joint and task spaces, respectively. $\mathbf{J} \in \mathbb{R}^{m\times n}$ is the Jacobian matrix. And the robots studied here are assumed not under-actuated, which yields $n \leq m$.

The manipulability ellipsoid and polytope have been systematically studied and compared as dexterity measurements for robot manipulators [12]. The manipulability ellipsoid can be obtained conveniently based on the l_2-norm estimation of the input velocities (namely $\|\dot{\boldsymbol{q}}\|_2 \leq 1$) as

$$\|\dot{\boldsymbol{q}}\|_2 = \dot{\boldsymbol{q}}^T\dot{\boldsymbol{q}} = \dot{\boldsymbol{y}}^T\mathbf{J}^{+T}\mathbf{J}^{+}\dot{\boldsymbol{y}} \leq 1 \tag{2}$$

where $\mathbf{J}^+ = \mathbf{J}^T(\mathbf{J}\mathbf{J}^T)^{-1}$ denotes the pseudo-inverse of the Jacobian matrix $\mathbf{J}$.

However, each active joint has its own velocity constraint in practice. Thus, the joint velocity vector will be confined within $\|\dot{\boldsymbol{q}}\|_\infty = \max|\dot{q}_i| \leq \dot{q}_{\max}$ rather than $\|\dot{\boldsymbol{q}}\|_2 \leq 1$. Therefore, the ellipsoid approach does not transform the exact velocity constraint from the joint space to the task space. Consequently, Lee [12] introduced the concept of the manipulability polytope as a more accurate and practical description of the dexterity for robot manipulators. And several concise methods [13] have been proposed to compute the corresponding polytope associated with the ∞-norm constraints of the active joints' input velocities.

Actually, the precision estimation for robot calibration suffers from the same problem. The robot's extended kinematic model can be generally expressed as

$$\boldsymbol{y} = \boldsymbol{f}(\boldsymbol{p},\, \boldsymbol{q}) \tag{3}$$

where $\boldsymbol{p}$ represent the kinematic-parameter vector.

Then, the linearized calibration model can be represented as

$$\Delta\boldsymbol{Y} + \varepsilon\boldsymbol{Y} = \mathbf{J}_P\Delta\boldsymbol{p} \tag{4}$$

where $\Delta\boldsymbol{Y} = [\Delta\boldsymbol{y}_1^T,\, \Delta\boldsymbol{y}_2^T,\, \cdots,\, \Delta\boldsymbol{y}_m^T]^T$ is the composed deviation of the measured poses $\boldsymbol{y}_i$ from their nominal ones $\hat{\boldsymbol{y}}_i$, namely $\Delta\boldsymbol{y}_i = \boldsymbol{y}_i - \hat{\boldsymbol{y}}_i, i = 1, 2, \cdots, m$. $\varepsilon\boldsymbol{Y} = [\varepsilon\boldsymbol{y}_1^T,\, \varepsilon\boldsymbol{y}_2^T,\, \cdots,\, \varepsilon\boldsymbol{y}_m^T]^T$ represents the composed random error vector during pose measurements. And $\Delta\boldsymbol{p}$ denotes the deviation of the kinematic parameters' actual values from their nominal ones. The identification Jacobian matrix is defined as $\mathbf{J}_P = [\mathbf{J}_{P,1}^T,\, \mathbf{J}_{P,2}^T,\, \cdots,\, \mathbf{J}_{P,m}^T]^T$, which can be obtained as

$$\mathbf{J}_{P,i} = \frac{\partial \boldsymbol{f}}{\partial \boldsymbol{p}}\bigg|_{\boldsymbol{y}=\hat{\boldsymbol{y}}_i},\ i = 1,\, 2,\, \cdots,\, m \tag{5}$$

Since the exact values of the measurement noise cannot be determined absolutely, the deviation of the parameters' actual values from their nominal ones can only be obtained according to the simplified form of Eq.4 as

$$\Delta\boldsymbol{Y} = \mathbf{J}_P\Delta\boldsymbol{p} \tag{6}$$

Comparing Eq.6 to Eq.4, it is obvious that the residual errors of the identified parameters satisfy the following relation.

$$\mathbf{J}_P \varepsilon \boldsymbol{p} = \varepsilon \boldsymbol{Y} \tag{7}$$

where $\varepsilon \boldsymbol{p} = \Delta \hat{\boldsymbol{p}} - \Delta \boldsymbol{p}^*$ denotes the residual errors, namely the difference between the identified values of the kinematic parameters from their actual ones.

Then, the estimation of the residual errors can be obtained as

$$\varepsilon \hat{\boldsymbol{p}} = \mathbf{J}_P^+ \varepsilon \boldsymbol{Y} \tag{8}$$

where $\mathbf{J}_P^+ = (\mathbf{J}_P \mathbf{J}_P^T)^{-1} \mathbf{J}_P^T$ is the Moore-Penrose inverse of $\mathbf{J}_P$.

All the aforementioned observability indices O_i $(i = 1, \cdots, 4)$ can be obtained based on the singular values of the identification Jacobian matrix $\mathbf{J}_P$ and related to some indices of the error ellipsoid, such as volume, eccentricity and maximum axis. Analogously, these results are derived under the assumption that the measurement error forms a hypersphere constraint, namely $\|\varepsilon \boldsymbol{Y}\|_2 \leq 1$. However, in practice the pose sensor performs the measurements independently at different configurations. As a result, the sensor noise will be bounded by $\|\varepsilon \boldsymbol{Y}\|_\infty = \max |\varepsilon y_i| \leq \varepsilon y_{i,max}$. Instead of the hypersphere, a hypercube can be obtained as the variable constraint (namely the domain) of Eq.8. According to the linear mapping of $\mathbf{J}_P$, a polytope will be derived as the range of the linear function. Obviously, it is the exact bound of the residual errors of the identified kinematic parameters, within which the real calibration errors will be confined.

Take the simple planar 2-R serial robot as an example. There are four kinematic parameters in this robot, namely the position of the fixed joint and the lengths of the links. To simplify the expression of discussion, but without loss of generality, only the length errors of the links are taken into consideration in this particular case.

Supposing three different configurations are measured for identifying the actual lengths of the links. For each configuration, a two-dimensional error vector is employed into the calibration model due to the sensor noise. Therefore, the total sensor noise will be constrained within a 6-hypercube. According to the linear mapping defined in Eq.8, the exact bound of the identified links' residual errors can be obtained in the form of a polygon, as illustrated in Fig.1.

From the figure, it is obvious that the exact error bound can be obtained as the convex hull of the image points mapped from the vertices of the measurement error's constraint hypercube. And most of the image points are transformed onto the inner points of the identified error polytope. The error ellipse is also illustrated in the figure for comparison. It shows that the error ellipse is smaller than the polygon both in volume and maximum magnitude. Additionally, the ellipse's maximum axis, known as the worst direction for error transmission, does not point to a certain vertex of the obtained error polygon. It means that the error ellipse just presents a qualitative evaluation for the residual errors and can not provide the quantitative estimation how accurate the kinematic parameters would be after identification. Thus, it can be stated that the polytope description is more direct and accurate than the ellipsoid one to evaluate the identification quality of the kinematic parameters.

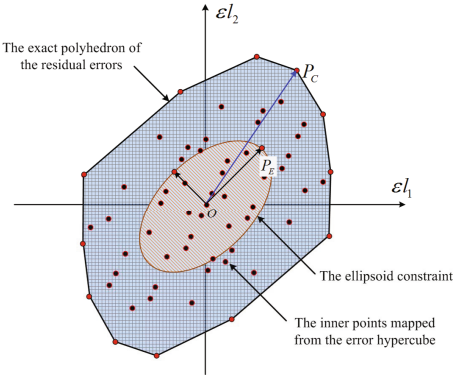

Fig. 1. Error polytope v.s. ellipsoid for the identified parameters

3 Observability Index Based on the l_∞-Norm Evaluation

As indicated in the above section, the precision estimation for robot calibration can be solved conveniently once the exact error bound of the identified parameters is determined absolutely. However, it is not an easy task to completely specify the error polytope due to the high dimension of the identified parameters and the excessive measurement datum.

Suppose the dimension of the robot's output vector is n and p kinematic parameters need to be calibrated with m different measured configurations. Then, the constraint of the measurement errors can be represented by a hypercube in the Euclidean space $\mathbb{R}^{mn}$. And the dimension of the identification Jacobian matrix satisfies $\mathbf{J}_P \in \mathbb{R}^{mn\times p}$. As a result, the problem of estimating the residual errors of the calibrated parameters has been transformed to the one of determining the error polytope in $\mathbb{R}^p$ mapped from the mn-hypercube through $\mathbf{J}_P$.

In the case of the six degree-of-freedom (DOF) Hexapod manipulator, there are totally 42 kinematic parameters to be calibrated and more than seven different configurations to be measured for reliable parameter identification [14]. The dimension of the composed error vector $\varepsilon \boldsymbol{Y}$ will be increased by six for each more measurement. Therefore, the least dimension of $\varepsilon \boldsymbol{Y}$ would be 48. Then, the total number of the vertices of the error hypercube will be $2^{mn} = 2^{48} \doteq 2.8147 \times 10^{14}$. Even for the kinematic parameter, the number of the error hypercube's vertices will exceed $2^p = 2^{42} \doteq 4.3980 \times 10^{12}$. It is an extremely big, even impossible, problem to completely determine the exact bound of the residual errors in such high dimension situation. Thus, it is necessary to define some indices to estimate the inaccuracy of the identified parameters.

As discussed in the above sections, the observability indices $O_i (i = 1, 2, 3, 4)$ are derived based on the 2-norm constraint for the measurement errors, as

$$\|\varepsilon \boldsymbol{Y}\|_2^2 = \varepsilon \boldsymbol{Y}^T \varepsilon \boldsymbol{Y} = \varepsilon \hat{\boldsymbol{p}}^T \mathbf{J}_P^T \mathbf{J}_P \varepsilon \hat{\boldsymbol{p}} = \varepsilon \hat{\boldsymbol{p}}^T \mathbf{M}_P \varepsilon \hat{\boldsymbol{p}} \leq 1 \tag{9}$$

where $\mathbf{M}_P = \mathbf{J}_P^T \mathbf{J}_P$.

As indicated in the literatures [15], the l_2-norm constraint is usually used in many robotics applications more because it is mathematically tractable than physically desirable. Since the pose sensor performs the measurement independently at different configuration during robot calibration, the l_∞-norm constraint is more practical than the l_2-norm one for the measurement errors.

Therefore, an alternative observability index is defined based on the ∞-norm of the identified parameters' residual errors as

$$O_\infty \triangleq \|\varepsilon \hat{\boldsymbol{p}}\|_\infty = \|\mathbf{J}_P^+ \varepsilon \boldsymbol{Y}\|_\infty \tag{10}$$

According to the definitions of the ∞-norm (the maximum row sum of absolute values) of vectors and matrices, the new index can be rewritten as

$$O_\infty = \max_{1\le i\le p} |\varepsilon \hat{\boldsymbol{p}}_i| = \max_{1\le i\le p} |\sum_{j=1}^{mn} (\mathbf{J}_P^+)_{i,j} \varepsilon \boldsymbol{Y}_j| \tag{11}$$

where $\varepsilon \hat{\boldsymbol{p}}_i$ and $\varepsilon \boldsymbol{Y}_j$ are the i^{th} and j^{th} components of the error vector $\varepsilon \hat{\boldsymbol{p}}$ and $\varepsilon \boldsymbol{Y}$ respectively. $(\mathbf{J}_P^+)_{i,j}$ denotes the entry in the i^{th} row and j^{th} column of $\mathbf{J}_P^+$.

For the vertices of the measurement error hypercube, the components of $\varepsilon \boldsymbol{Y}$ would be either 1 or -1 (namely $\varepsilon \boldsymbol{Y}_j = \pm 1$). Let $\varepsilon \boldsymbol{Y}_j$ have the same sign as the entry $(\mathbf{J}_P^+)_{i,j}$. Then, the observability index can be finally determined as

$$O_\infty = \max_{1\le i\le p} |\varepsilon \hat{\boldsymbol{p}}_i| = \max_{1\le i\le p} \sum_{j=1}^{mn} |(\mathbf{J}_P^+)_{i,j}| = \|\mathbf{J}_P^+\|_\infty \tag{12}$$

From Eq.12, O_∞ can be simply the l_∞-norm of $\mathbf{J}_P^+$. Its physical meaning is the maximum absolute value of the components in the identified parameters' residual errors. For a given planar vector $\boldsymbol{r}_p = (x_p, y_p)^T$, the ∞-norm produces a square constraint with the side equal to the maximal component of the vector, namely $\|\boldsymbol{r}_p\|_\infty = \max\{|x_p|, |y_p|\}$. Using this concept, Eq.8 can be interpreted in a geometric manner. Still take the planar case as an example. As shown in Fig.2, based on the image points transformed from the measurement errors' constraint hypercube, different estimations for the error bound of the identified parameters can be obtained according to different criterions.

On one hand, a circular area can be obtained according to the l_2-norm evaluation. From the figure, it is obvious that this circle is inscribed by the exact error polygon. Based on this criterion, it can be guaranteed that the l_2-norm values of the residual errors will not exceed the radius of the bounding circle. It sounds a reasonable evaluation for the inaccuracy of the kinematic parameters for robot calibration. However, it is difficult to identify the vertex with maximum l_2-norm in high dimensional cases, such as the spatial parallel manipulators.

On the other hand, a square region can also be obtained based on the l_∞-norm evaluation of the residual errors, as shown in the figure. The physical meaning of this estimation is that each component of the residual errors will not be larger than this magnitude. And it is easy to calculate the side length of this bounding square according to Eq.12. Moreover, a smaller bounding box can be specified by

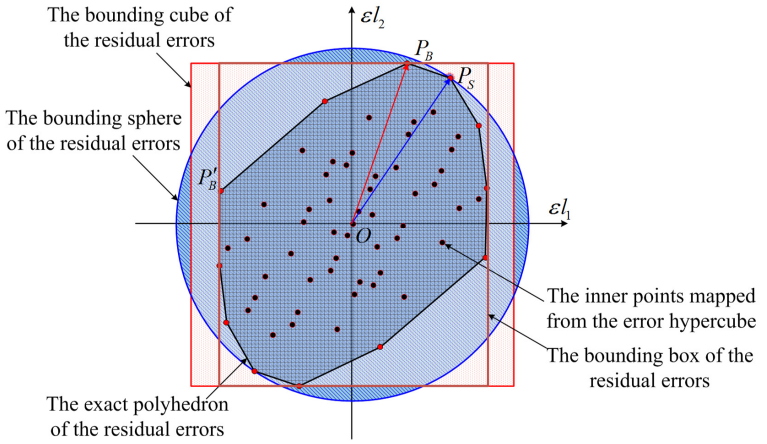

Fig. 2. Comparison of the 2-norm and infinity-norm evaluations for the residual errors

computing each row sum of absolute values of $\mathbf{J}_P^+$, namely the l_1-norm of the row vectors, which binds the residual errors. As a result, for a given matrix $\mathbf{J}_P^+$ there exist individual assessments for the error bound of all identified parameters. And the observability index O_∞ is defined as the largest one for the overall evaluation of the identification inaccuracy.

4 PSO Algorithm with Collision Mechanism

In this section, the PSO algorithm [16,17] is introduced to search for the optimal configuration set according the observability index O_∞. Taking the active joints' boundary constraints into account, a collision-mechanism is employed into the standard PSO algorithm to cope with boundary constraint problem.

The actual position of one particle in the swarm is associated with a particular design vector $\boldsymbol{x}$, the dimension of which equals to the number of design variables in the studied problem. The trajectory of the i^{th} particle at iteration k can be described with the position update equation as

$$\boldsymbol{x}_i^{k+1} = \boldsymbol{x}_i^k + \Delta\boldsymbol{x}_i^{k+1} \tag{13}$$

where the velocity update equation for the particle can be determined as

$$\Delta\boldsymbol{x}_i^{k+1} = \omega\Delta\boldsymbol{x}_i^k + c_1 r_{1,i}^k(\boldsymbol{x}_i^{b,k} - \boldsymbol{x}_i^k) + c_2 r_{2,i}^k(\boldsymbol{x}_*^{b,k} - \boldsymbol{x}_i^k) \tag{14}$$

where $\boldsymbol{x}_i^{b,k}$ denotes the best previously obtained position of the particle i before the current iteration and $\boldsymbol{x}_*^{b,k}$ is the previously best one among the entire swarm. The random numbers $r_{1,i}^k$ and $r_{2,i}^k$ are uniformly distributed in [0, 1]. c_1 and c_2 are referred to as the intelligent particles' cognitive and the social scaling factors. And ω denotes the inertia factor.

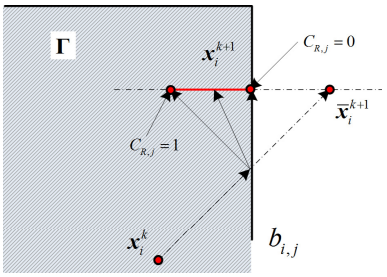

Fig. 3. The collision mechanism of PSO algorithm

Applying the algorithm to our problem, each particle among the swarm corresponds to a set of measurement configurations. Then, the problem can be set up conveniently and the updating theme of the swarm can be implemented readily. However, the standard PSO algorithm is usually applied to solve unconstrained optimization problems. In order to handle the motion constraint of the robot's active joints, a collision-mechanism is introduced to maintain a feasible population when some particles cross across the searching boundary.

Suppose the particles are constrained within the feasible searching region $\mathbf{\Gamma}$, as shown in Fig.3. Then, a collision will occur when the updated position of a particle reaches outside. It is natural and intuitive to regard $\mathbf{\Gamma}$ as a cage made of glass. Although the particles are with intelligence, they cannot realize the existence of the transparent boundary. When they find better positions based on their cognitive and social intelligence, they will fly towards them without any hesitation. Then, infeasible individuals will be generated among the population if no handling strategy is introduced.

The basic idea of the collision-mechanism is based on the inelastic behavior of two colliding objects. The searching particles are supposed to be bounced back when they hit the boundary of $\mathbf{\Gamma}$. Then, the position update theme of the flying particles can be rewritten as follows if collision happens.

$$\boldsymbol{x}_{i,j}^{k+1} = b_j - C_{R,j}\left(\boldsymbol{x}_i^k + \Delta\boldsymbol{x}_{i,j}^{k+1} - b_j\right) \tag{15}$$

where b_j represents the limitation of the j^{th} component of the design vector $\boldsymbol{x}$. And $0 \leq C_{R,j} \leq 1$ is the coefficient of restitution. $C_{R,j} = 0$ and $C_{R,j} = 1$ are associated with the perfectly inelastic and elastic collisions, respectively.

Based on the modified updating theme, the evolving population will search the best position for the particles within the feasible region all the time to guarantee the algorithm proceed successfully. Additionally, the restitution coefficient can be modified flexibly between 0 and 1 in different cases. As pointed by Nategh [14], the maximum observability index is potentially obtained at the extreme boundary of the robots' motion constraints. Then, for our optimal configurations selection problem, the collisions are supposed to be perfectly inelastic ones, namely $C_{R,j} = 0$, to make the algorithm quickly converge.

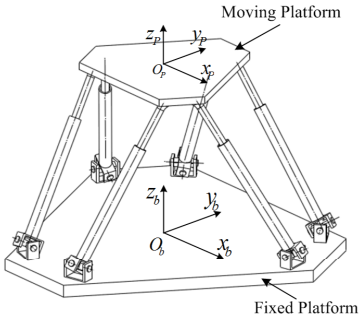

Fig. 4. The hexapod (6-UPS) parallel manipulator

5 Numerical Simulations

In this section, the hexapod (6-UPS) parallel manipulator, as shown in Fig.4, is studied as a numerical example to demonstrate the proposed calibration method. There are 7 independent kinematic parameters to be identified in each limb, namely the position vector of the universal joint on the fixed platform $\boldsymbol{u}_i$, the initial length of the prismatic joint l_i and the position of the spherical joint on the moving platform $\boldsymbol{s}_i$. Thus, there are totally 42 parameters to be identified during the kinematic calibration, whose nominal values are listed in Tab.1.

Each measurement generates six constraint equations to the calibration system. Therefore, at least 8 measurement configurations are required for reliable parameter identification. In order to reduce the influence of the sensor noise, 14 different configurations are measured. The pose sensor's measurement errors are assumed to be uniformly distributed in $\varepsilon_p \in [-0.010,\ 0.010]\, mm$ for position and $\varepsilon_o \in [-0.001,\ 0.001]\, rad$ for orientation. Otherwise, the motion ranges of the actuated prismatic joints lie in $q_i \in [-200.00, 200.00]\, mm, i = 1, \cdots, 6$.

Using the modified PSO algorithm, the optimal measurement configurations for kinematic calibration can be determined conveniently based on the proposed observability index O_∞ whose iterative improvement is illustrates in Fig.5. From

Table 1. Nominal values of kinematic parameters (mm)

Limb No.	$\boldsymbol{u}_i$	l_i	$\boldsymbol{s}_i$
1	$(1931.8517,\ 517.6381, 0)^T$	3757.4884	$(565.6854,\ 565.6854, 0)^T$
2	$(-517.6381,\ 1931.8517, 0)^T$	3757.4884	$(207.0552,\ 772.7407, 0)^T$
3	$(-1414.2136,\ 1414.2136, 0)^T$	3757.4884	$(-772.7407,\ 207.0552, 0)^T$
4	$(-1414.2136, -1414.2136, 0)^T$	3757.4884	$(-772.7407, -207.0552, 0)^T$
5	$(-517.6381, -1931.8517, 0)^T$	3757.4884	$(207.0552, -772.7407, 0)^T$
6	$(1931.8517,\ -517.6381, 0)^T$	3757.4884	$(565.6854, -565.6854, 0)^T$

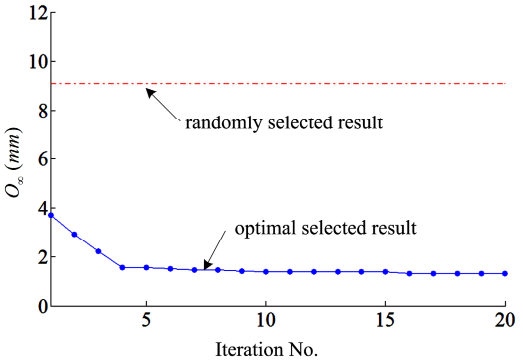

Fig. 5. Improvement of the observation index O_∞ during the searching process

the figure, it is obvious that the observability index is reduced significantly by the properly selected configurations than that by the random ones.

In order to validate the obtained result, numerical simulations are carried out. Random errors ranged in $[-5.0, 5.0]\,mm$ are added to the nominal parameters to obtain the presumed actual ones. The robot's simulated actual poses is obtained by means of a numerical method to the forward kinematics analysis. Additionally, uniformly distributed measurement errors are introduced to simulate the sensor noise.

As shown in Fig.6, the residual errors of the robot's identified parameters are much smaller than the manufacturing and assembly tolerances before calibration. Moreover, the identification precision can be further improved by choosing a set of optimal measurement configurations. In the numerical example, mean value of the residual errors has been reduced from $0.370\,mm$ to $0.047\,mm$.

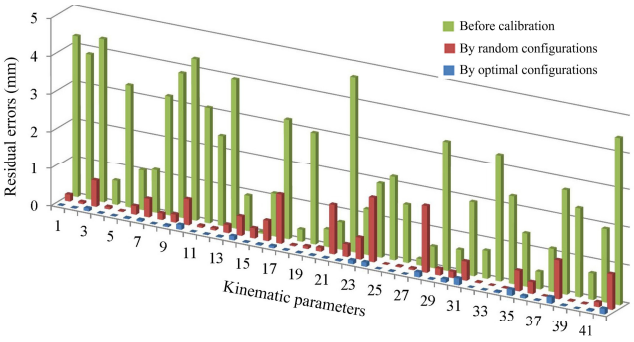

Fig. 6. Residual errors of the identified parameters

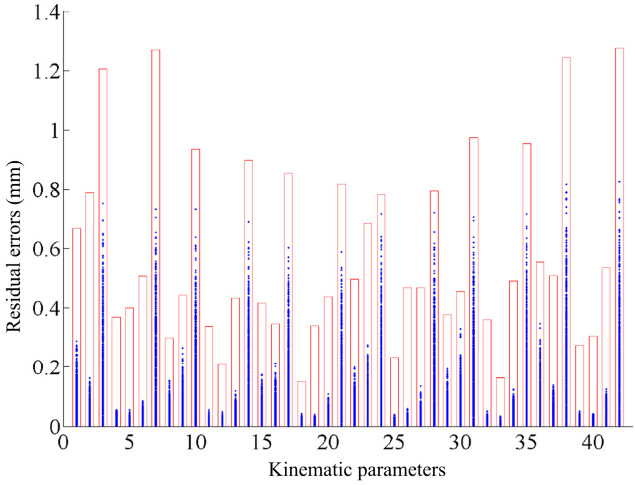

Fig. 7. Residual errors of the identified parameters in numerical experiments

Otherwise, the boundary for all parameters' residual errors can also be obtained by calculating all rows' l_1-norm of $\mathbf{J}_P^+$, which can be regarded as a threshold for identification inaccuracy. To verify this property, another numerical experiment is designed by repeating the above calibration simulation for thousands of times, as shown in Fig.7. It is evident that none of the maximal residual errors of the identified parameters exceeds this theoretical maximum. But in some cases, the maximal residual errors are close to this threshold, which means that the worst situation for parameter-identification may arise due to unfortunate distribution of the random measurement errors for the end-effector's poses. Therefore, the final accuracy performance of the calibrated manipulator can be obtained with this estimation for the parameters' identification inaccuracy.

6 Conclusion

In this paper, a new observability index is proposed for the optimal configurations selection for robot calibration. The concept of the error polytope is introduced to describe the inaccuracy of the identified parameters based on the l_∞-norm evaluation, which provides a deterministic estimation for residual errors. The new index is not only mathematically tractable but also with intuitive physical meanings. It has ascertained the absolute bound of the potential residual errors and then guaranteed the identification inaccuracy not exceed some specific thresholds. The results of the numerical simulation have verified the correctness and effectiveness of the proposed approach.

Acknowledgments. This research work is supported by the National Science Foundation of China (NSFC) under Grant No. 51075259 and 51121063.

References

1. Mooring, B., Roth, Z., Driels, M.: Fundamentals of Manipulator Calibration. John Wiley & Sons (1991)
2. Driels, M., Pathre, U.: Significance of observation strategy on the design of robot calibration experiments. Journal of Robotic Systems 7(2), 197–223 (1990)
3. Borm, J., Meng, C.: Determination of optimal measurement configurations for robot calibration based on observability measure. International Journal of Robotics Research 10(1), 51–63 (1991)
4. Khalil, W., Gautier, M., Enguehard, C.: Identifiable parameters and optimum configurations for robot calibration. Robotica 9(1), 63–70 (1991)
5. Zhuang, H., Wang, K., Roth, Z.: Optimal selection of measurement configurations for robot calibration using simulated annealing. In: 1994 IEEE International Conference on Robotics and Automation, pp. 393–398 (1994)
6. Daney, D., Papegay, Y., Madeline, B.: Choosing measurement poses for robot calibration with the local convergence method and tabu search. International Journal of Robotics Research 24(6), 501–518 (2005)
7. Verl, A., Boye, T., PottD, A.: Measurement pose selection and calibration forecast for manipulators with complex kinematic structures. CIRP Annals-Manufacturing Technology 57(1), 425–428 (2005)
8. Menq, C., Borm, J., Lai, J.: Identification and observability measure of a basis set of error parameters in robot calibration. Journal of Mechanical Transmission, Automation Design 111(4), 513–518 (1989)
9. Nahvi, A., Hollerbach, J.: The noise amplification index for optimal pose selection in robot calibration. In: 1996 IEEE International Conference on Robotics and Automation, pp. 647–654 (1996)
10. Nahvi, A., Hollerbach, J., Hayward, V.: Calibration of a parallel robot using multiple kinematic closed loops. In: 1994 IEEE International Conference on Robotics and Automation, pp. 407–412 (1994)
11. Sun, Y., Hollerbach, J.: Observability index selection for robot calibration. In: 2008 IEEE International Conference on Robotics and Automation, pp. 831–836 (2008)
12. Lee, J.: A study on the manipulability measures for robot manipulators. In: 1997 IEEE International Conference on Intelligent Robots and Systems, pp. 1458–1464 (1997)
13. Hwang, Y., Lee, J., Hsia, T.: A recursive dimension-growing method for computing robotic manipulability polytope. In: 2000 IEEE International Conference on Robotics and Automation, pp. 2569C–2574C (2000)
14. Nategh, M., Agheli, M.: A total solution to kinematic calibration of hexapod machine tools with a minimum number of measurement configurations and superior accuracies. International Journal of Machine Tools and Manufacture 49(15), 1155–1164 (2009)
15. Shim, I., Yoon, Y.: Stabilized minimum infinity-norm torque solution for redundant manipulators. Robotica 16(2), 193C–205C (1998)
16. Kennedy, J., Eberhart, R.: Particle swarm optimization. In: 1995 IEEE International Conference on Netual Network, pp. 1942–1948 (1995)
17. Coath, G., Halgamuge, S.: A comparison of constraint-handling methods for the application of particle swarm optimization to constrained nonlinear optimization problems. In: 2003 IEEE Congress on Evolutionary Computation, pp. 2419–2425 (2003)